Journal of Environment and Earth Science
ISSN 2224-3216 (Paper) ISSN 2225-0948 (Online)
Vol.16, No.1, 2026 

# Petrogenetic Characterization of Talcose Rocks of Ibogunde, Southwestern Nigeria, West Africa

*Alao-Daniel, A. B.[1, 2], Adetunji, A.[1] and Eruteya,O. E.[3]
[1] Department of Geology, Obafemi Awolowo University, Ile-Ife, Nigeria
[2] Department of Earth Sciences, University of Western Cape, Belleview, South Africa
[3] Department of Geology, University of Geneva, Switzerland
*Corresponding Author: adedamolaalaodaniel@oauife.edu.ng

**ABSTRACT**
Geological mapping on a scale of 1:12,500, mineralogical and geochemical studies of talcose rocks in Ibogunde, Southwestern Nigeria were carried out in order to account for these industrial minerals and to decipher the petrogenesis. Whole-rock major element compositions of eleven (11) talcose and five (5) quartzite rock samples were determined using a PANalytical Axios Wavelength Dispersive spectrometer while the trace and rare earth elements were analysed by LA-ICP-MS (Laser Ablazer Inductively Coupled Mass Spectrometer) at the Central Analytical Facilities, Stellenbosch University, South Africa. Powders of representative talcose rocks were examined for routine qualitative mineral identification using D8-Advance Brunker X-Ray diffractometer at iThemba Lab, Capetown, South Africa. The talcose rocks occurred as small bodies within quartzite in the study area. Under the microscope, it consists of minerals that are bent which are indicative of deformation. Some grains showed radiating textures while others showed parallel alignment of longer axes in preferred orientation. The geochemical result showed higher mean compositions of $SiO_2$ as 60.12 wt. %; moderate $Al_2O_3$ (1.19 wt. %); $Fe_2O_3$ (4.83 wt. %). MgO has generally high value between 25.31 and 29.13 wt. % with an average of 27.59 wt. %. The ratios for $La_n/Yb_n$, $La_n/Sm_n$ and $Ce_n/Yb_n$ ranged from 2.5 to 22.77, 2.53 to 5.94 and 1 to 23.33, respectively indicated fractionation of the source magma (komatiite). Ni and Cr have high mean concentrations of 1880.45 ppm and 3236 ppm, respectively; which were deduced to be as a result of immobility of these trace elements even under hydrothermal alteration. The results of the X-ray diffraction analysis of the samples showed peaks for talc, chlorite and tremolite. Ternary discrimination plots indicate that the talcose rocks were products of metamorphism of komatiite.
**Keyword**: Petrogenesis, Talcose rocks, Komatiite, Geochemical.
**DOI:** 10.7176/JEES/16-1-05
**Publication date:** March 28th 2026

## 1. INTRODUCTION

Talc is a hydrothermal alteration product of basic and ultrabasic rocks (Hess, 1993) and is essentially a hydrous magnesium silicate with chemical formula $MgSi_3O_8$ (OH). It belongs to a subclass of phyllosilicates (Fig. 1). It is not soluble in water, but is slightly soluble in dilute mineral acids. Its colour ranges from white to grey or green and it has a distinctly greasy feel with white streak (Luzenac, 2006).
Talc has been reported in at least twenty-five (25) localities in Nigeria with an estimated reserve of over 100 million tonnes (Adekoya, 1999). The more important occurrences are located at Ilesa (Elueze and Ogunniyi, 1985), Apomu-Ife (Ige, 1987), Iseyin District (Elueze and Awonaiya, 1989), Asegbo in Ilesa, Obaluru-Araromi (Akin-Ojo, 1992); Kumanu, Assaya and Yarada in Niger State, Odogbe in Kwara State, Oke-Ila (Bolarinwa, 2001), Baba-Ode (Okunlola *et al.,* 2002), Igbo Igbon (Ayemo, 2003), Erin-Omu (Okunlola and Anikulapo, 2006); Esie in Kwara State (Olorunfemi *et al.,* 2009), Ijero-Ekiti (Okunlola *et al.,* 2011), Wonu-Laduntan in Apomu area (Bolarinwa and Adeleye, 2015) and Itagunmodi-Igun (Olajide-Kayode *et al.,* 2018). Nigeria talc has its largest economic deposits in Kamanu, Odogbe in Niger and Kwara States, respectively (Durotoye and Ige 1991; Adekoya, 1999). Due to the fact that it rarely occurs pure but in association with other minerals in varying proportions, it is therefore described as talcose rocks.

 

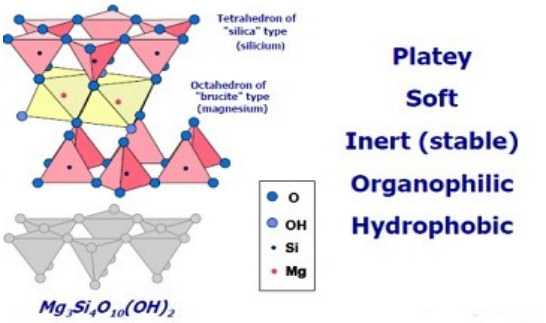


**Figure 1: Talc Crystal structure (Luzenac, 2006)**

Geological mapping done in Ibogunde and environs by Geological Survey of Nigeria was on a smaller scale of 1:250,000. The most recent update of the geological map was carried out by Department of Geology of the Obafemi Awolowo University, Ile-Ife on a scale of 1:50,000 during the recently concluded University Assisted Program sponsored by Exxon Mobil Limited. However, these scales could not account for small industrial mineral bodies in the area.
There is therefore a need to carry out geological mapping on a scale of 1:12,500 or larger on which these small rock bodies and minerals could be accounted for. It is also pertinent to examine the mineralogy and chemistry of the talcose rocks to establish their genetic origins. Also, the occurrence and the origin of Ibogunde talcose rocks have not been formally documented or published in any literature.

### 1.1 *Location and accessibility*

The spatial framework of the study area is based on Global Reference Network (GRN) cells defined by Darnley *et al.* (1995) and falls within N05 E04 GRN cell (Fig. 2). It falls within the Iwo S. E. and N. E. standard topographic sheets number 242 (1:50,000) published by the Federal Survey of Nigeria in 1965. These were later enlarged to 1:12,500. The total area covered is about 14.8 km by 11.2 km defined by latitudes 7° 42' and 7° 50' N and longitudes 4° 18' and 4° 24' E (Fig. 3).

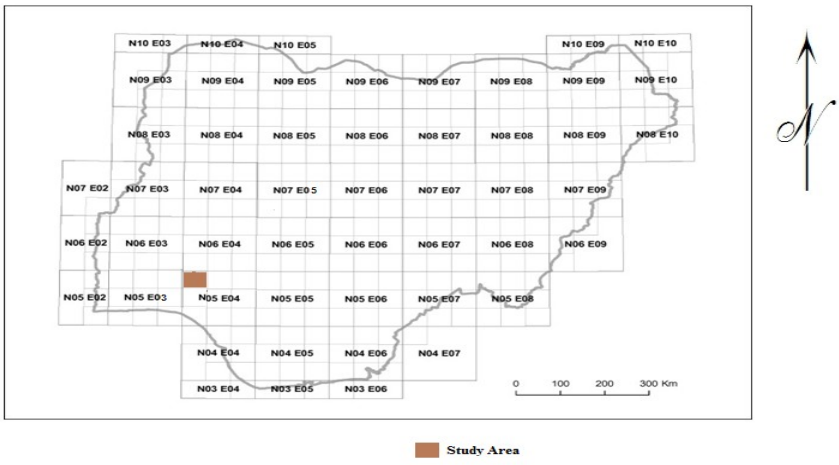


**Figure 2: The Distribution of Global Refernce Network (GRN) Cells in Nigeria (Darnley *et al.*, 1995)**

 

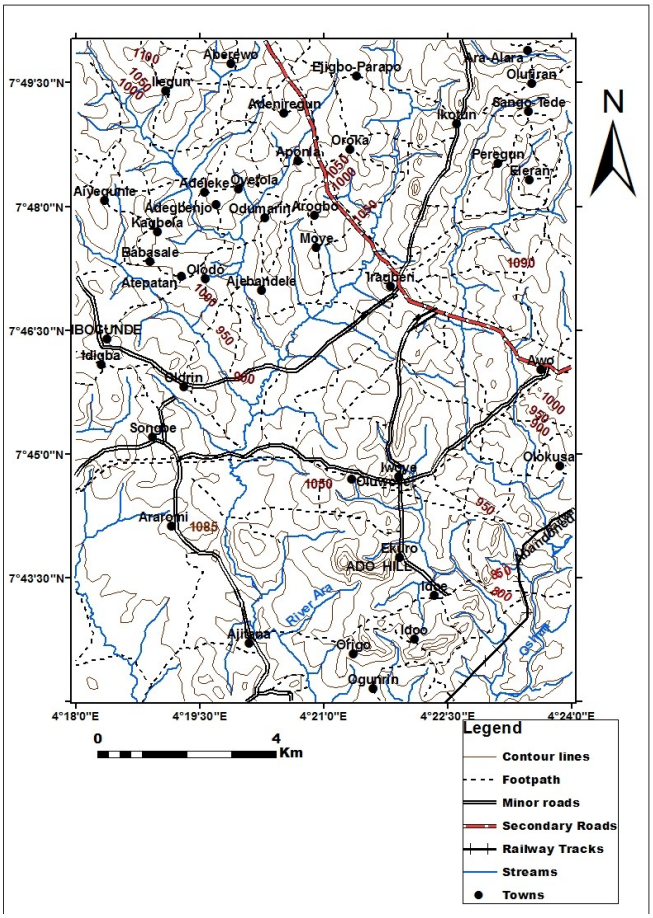


**Figure 3: Topographical Map of the Study Area (Culled from Iwo Sheets 242 S. E. and N. E., Federal Survey of Nigeria, 1965)**

### 1.2 *Relief and topography*

Several relief and topographic features characterize the study area and they show strongly contrasting features. The highest point is 332 m above mean sea level, which is found at Idoo, west of Ede. The lowest portion is 244 m above sea level that falls within the hill of River Edero to the north-central. The topography is largely dominated by pediplains with isolated hills around Origo, Osuntedo and Ekuro. There is also a prominent ridge (with very small width) which trends from north through Iragberi to Iwoye.

## 2. REGIONAL GEOLOGICAL SETTING

The study area located in Southwestern Nigeria is underlain by rocks of the Basement Complex of Nigeria, which forms part of the Pan African mobile belt. The Basement terrane is situated between the West African Craton to the west and Congo Craton to the southeast and southwest of Saharan block (Fig. 4). It occupies part of the area refer to as Benino-Nigeria shield which is the southern part of Trans Saharan fold belt. The north of the belt is made up Pharussian belt to east west, LATEA at the center and East Hoggar to the east. Southwards is the Aïr shield (Figure 4). The Nigeria sector of the Benino-Nigerian shield is made up of two terranes: low grade western Nigeria terrane that is largely greenschist-amphibolite grade metamorphism with pockets of granulite facies and medium-high grade metamorphic eastern Nigeria terrane which is largely granulite facies.

 

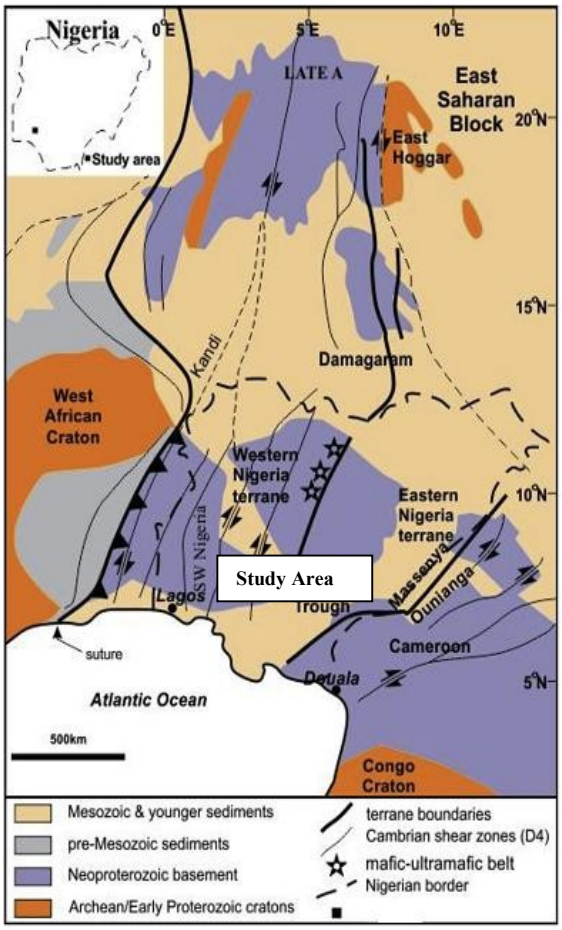


**Figure 4: Geological Sketch Map of the Pan-African Mobile Belt (modified from Ajibade and Wright, 1989; Caby, 1989; Black *et al.*, 1994; Liegeois *et al.*, 1994; Ferre *et al.*, 1996; Ferre *et al.*, 2002; Adetunji *et al.*, 2016)**

Rahaman (1976, 1988) classified the Basement Complex rocks of Nigeria into six major groups and this scheme was used in this study: Migmatite-Gneiss-Quartzite Complex; slightly migmatized to non-migmatized metasedimentary and meta-igneous rock also referred to as newer metasediments (Oyawoye, 1964) or Schist Belt (Ajibade, 1976; Turner, 1983); charnockitic, gabbroic and dioritic rocks.; members of the Older Granite suite; metamorphosed to unmetamorphosed calc-alkaline volcanics and hypabyssal rocks (Mc Curry, 1976); unmetamorphosed dolerite dykes, basic dykes and syenite dykes etc.

### 2.1 *Geology of the area*

Locally, the geology of the area consists of grey gneiss, quartzite, granite gneiss, charnockitic rocks (of various textural characteristics and composition) and diorite (Fig. 5). Grey gneiss occupies the low topographic areas. It is found between Awo and Iwoye areas. The rock is light grey and characterized by well-defined lithological banding. The bands are made up of alternation of light and dark coloured bands. The widths of these bands vary (0.2 - 3 cm). Quartzite forms a narrow, slightly elevated topography that trend north-south in the eastern part of the study area. It occurs mainly as low-lying exposures. Then quartzite band extends from eastern part of Idoo through Iwoye and Iragberi. This is the structural marker in the study area with an antiformal fold which runs north-south

 

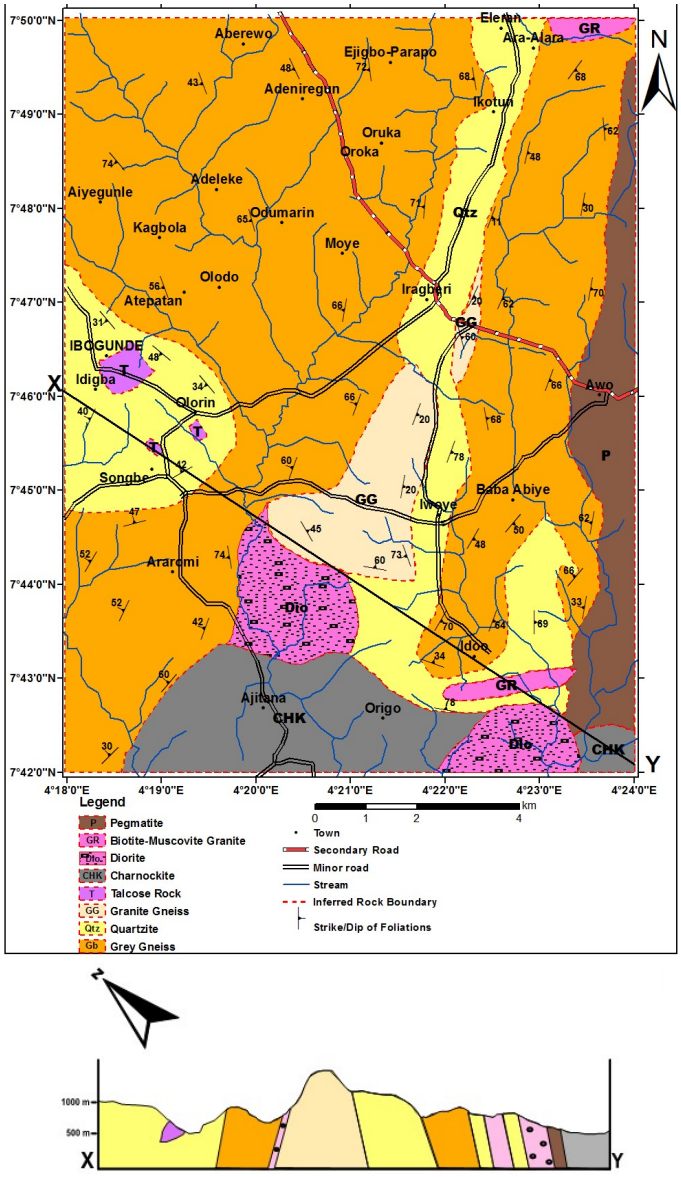


**Figure 5: Geological Map and Cross Section of Ibogunde and its Environs (Adapted from Owoeye, 2020)**

and refolded at the base to give a synform. The granite gneiss occupies areas of relatively high elevations in the area which falls around Awo and Iwoye and major quarries (Tewo and Wolid quarries at Iwoye as large, hilly and extensive exposures) in the study area.

The rock is mostly light pink in colour; sometimes greyish. It is coarse grained with dominant quartzo-feldspathic minerals. Charnockite is exposed generally in the southern part of the studied area. Most of the outcrops are low lying. It outcrops as small plutons in Osuntedo, Ajitenna and bouldery units in Awo. Fresh samples are dark green in colour while the weathered sample has a dark brown colour. It is slightly dark green due to the presence of two pyroxenes (clinopyroxene and orthopyroxene) and amphibole. Diorite has a dome-like occurrence in the southeastern part of the study area around R.T.O. Farm; it occurs as a circular body around Origo station and southeast of Idoo village. The rock is light grey in colour. It is medium to coarse grained in texture. Pegmatite occurs as intrusive igneous rocks in the granite and grey gneisses. It covers the extreme eastern part of the study area and was also found at the Origo hill. The pegmatite at Aba Alaye, though not on a mappable scale, is zoned with well-formed quartz and feldspar crystals segregated. The rock occurs basically within all the various rock types mapped within the study area. It has contact with quartzite, grey gneiss and charnockite. The hand specimen contains giant crystals of feldspars, quartz, black tourmaline and books of

 

micas. Biotite-muscovite granite occurs in the study area as minor intrusives in form of tabular bodies and is mainly low lying. They were encountered around Afaake and Inisa - Edoro. A more detailed geology of the area is discussed in Owoeye (2020) and Alao-Daniel *et al.* (2023).

## 3. METHODOLOGY

Eleven representative samples of talcose rocks were collected during the geological mapping done on a scale of 1:12,500. Equally, samples of enclosing rock (quartzite) were also collected for analyses. Thin sections of the talcose samples were prepared at the Workshop in the Department of Geology, Obafemi Awolowo University, Ile-Ife. These were studied with polarizing microscope to determine microstructures and other silicate minerals present. The minerals were identified using their optical properties and photomicrographs showing particular textural features were also taken for emphasis.

About 10 g of each talcose and quartzite samples were crushed into a fine powder (particle size < 70 µm) with a jaw crusher and milled in a tungsten-carbide Zibb mill at the Central Analytical Facilities at the Department of Geology, Stellenbosch University, South Africa prior to the preparation of a fused disc for major and trace elements analyses. The jaw crusher and mill were cleaned with clean uncontaminated quartz between two (2) samples to avoid cross contamination. Glass disks were prepared for XRF analysis using 7 g of high purity trace element and Rare Earth Element-free flux ($LiBO_2$ = 32.83%, $Li_2B_4O_7$ = 66.67%, LiI = 0.50%) mixed with 0.7 g of the powdered sample. Mixtures of the sample and flux were fused in platinum crucibles with Claisse M4 gas fluxer at temperatures between 1100 °C - 1200 °C.

Whole-rock major element compositions were determined by XRF on a PANalytical Axios Wavelength Dispersive spectrometer at the Central Analytical Facilities, Stellenbosch University, South Africa. The spectrometer was fitted with a Rhodium tube and with the following analyzing crystals: LIF200, LIF220, PE 002, Ge 111 and PX1. The instrument was fitted with a gas-flow proportional counter and a scintillation detector. The gas-flow proportional counter used a 90% Argon – 10% methane mixture of gases. Major elements were analyzed on a fused glass disk using a 2.4 kW Rhodium tube. Matrix effects in the samples were corrected for by applying theoretical alpha factors and measured line overlap factors to the raw intensities measured with the SuperQ PANalytical software. The concentration of the control standards that were used in the calibration procedures for major element analyses fit the range of concentration of the samples. Amongst these standards were NIM-G (Granite from the Council for Mineral Technology, South Africa) and BE-N (Basalt from the International Working Group).

For LA-ICP-MS, fusion disks prepared for XRF analysis by an automatic Claisse M4 Gas Fusion instrument and ultrapure Claisse Flux, using a ratio of 1:10 sample : flux, were coarsely crushed and a chip of sample mounted along with up to 12 other samples in a 2.4 cm round resin disk. The instrumental method set-up followed the guidelines from Eggins (2003). A Resolution 193 nm Excimer laser from ASI connected to an Agilent 7700 ICP-MS was used in the analysis of trace. Ablation was performed in He gas at a flow rate of 0.35 L/min, then mixed with argon (0.9 L/min) and Nitrogen (0.004 L/min) just before introduction into the Inductively Coupled Plasma. For trace elements in fusions, the fused samples were laser ablated on each sample using a frequency of 10 Hz and fluence of ~6 J/cm$^2$. NIST 610 glass (values from Jochum *et al.,* 2011) was used for quantification and analysed every 15 samples, along with BCR-2G and BHVO-2G (values from GeoReM: Jochum *et al.,* 2005). A fusion control standard from certified basaltic reference material (BCR-2, and BHVO-1, values from Jochum *et al.,* 2016) was also analysed in the beginning of a sequence to verify the effective ablation of fused material. Data processing was done using the LA-ICP-MS data reduction software package Iolite v.3.2 (Paton *et al.,* 2011).

The whole-rock geochemical data of the representative samples were interpreted using various discrimination diagrams that were generated with GCDkit software.

Powders of ten (10) representative talcose rocks were examined for routine qualitative mineral identification to compliment the petrographical studies. This was carried out at iThemba Lab, Capetown, South Africa. Measurements were performed using a multi-purpose X-ray diffractometer D8-Advance from Bruker operated in a continuous θ-θ scan in locked coupled mode with Cu-Kα radiation ($\lambda K\alpha_t$=1.5406Å). Each sample was mounted in the centre of the sample holder on a glass slide and levelled up to the correct height. The measurements were run within a range in 2θ defined by the user with a typical step size of 0.025 ° in 2θ. A position sensitive detector, Lyn-Eye, was used to record diffraction data at a typical speed of 0.5 sec/step which is equivalent to an effective time of 92 sec/step for a scintillation counter.

Other instrumental settings are:
Wavelength: 0.15406 nm
Power: 40 kV 40 mA
Optical geometry: Bragg-Bretano
Step size: 0.025 degree/step
Exposure time: 0.1 s/step

 

Tube voltage: 40 kV
Tube current: 40 mA
Variable slits: variable slit
2θ Range available: 0.5° to 130°
For the phase analysis to be carried out for diffraction pattern with zero background after the selection of a set of possible elements from the periodic table, data were background subtracted. Phases were identified from the match of the calculated peaks with the measured ones until all phases were identified within the limits of the resolution of the results. The software used was from International Center of Diffraction Data (ICDD) database (2017) for Powder Diffraction File (PDF). The data evaluation was done with EVA software from Bruker. The percentage of each mineral per sample was also calculated. The text files of as-measured and background subtracted data in (2theta, Intensity) was plotted with Origin software and each identified phase was appropriately labelled.

## 4. RESULTS AND INTERPRETATION

Talcose rocks in the study area are predominantly low-lying exposures. They occur as small aggregate of boulders that are discontinuous over the area (Fig. 6a) as indicated in the geological map (Fig. 5); some are found within laterites (Fig. 6b). They generally occur within weathered quartzite (Fig. 6c); some varieties are weakly foliated as shown in Figure 6d while some show radiating textures (Fig. 6d).


**Figure 6: Field photographs showing bouldery exposure (a), talcose rock in laterite (b) within quartzite (c); foliated (d) weakly foliated talcose rock**

Microscopically, the talcose rocks consist of predominantly colourless minerals that show fibrous, radiating and platy textures (Fig. 7a). Some of the platy and fibrous grains show parallel arrangements of longer axes in preferred orientation. The minerals also occur in shreds that are bent, which may be indicative of plastic deformation (Fig. 7b). In addition to talc, the rock is composed of chlorite and some opaque minerals. There is also occurrence of zircon as minor constituent. The zircon crystals are euhedral with rims of pleochroic halos which is essentially of radioactive elements in the zircon (Fig. 7c).
Chlorite is seen as net-like crystals within the talc matrix. It is greenish in colour and is strongly pleochroic in shades of green and brown. It exhibits parallel extinction.

 

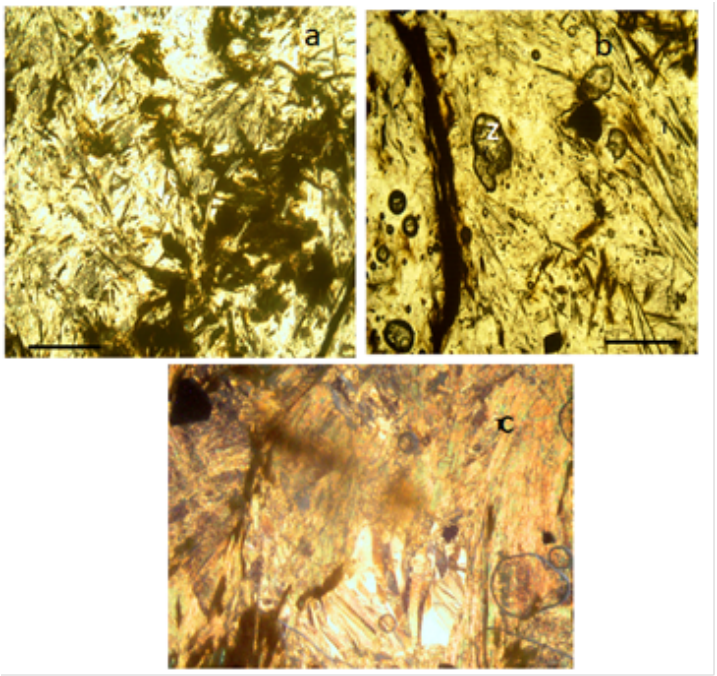


**Figure 7: Photomicrographs of talcose rock with radiating texture (a), bent grains (b) and foliated texture (c) and zircon (z)**

The results of the geochemical analyses for the talcose rocks are presented in Table 1. The REE values were normalized to that of chondrite using the values of McDonough and Sun (1995). As shown in Table 1, the rock is characterized by small range of composition of $SiO_2$ between 57.96 and 61.69 wt. % (with mean of 60.118 wt. %); low concentration of $TiO_2$ from 0.02 to 0.07 wt. % with an average of 0.035 wt. %; moderate $Al_2O_3$ ranging from 0.37 to 2.68 wt. % (mean of 1.19 wt. %); moderate $Fe_2O_3$ between 3.95 and 5.73 wt. % with an average of 4.83 wt. %. The values of $Cr_2O_3$ range between 0.21 and 0.95 wt. % with a mean of 0.593 wt. %; low MnO ranging from 0.05 to 0.10 with a mean of 0.074wt. %. MgO has generally high value between 25.31 and 29.13 wt. % with an average of 27.59 wt. %. The rock generally has low to moderate CaO (0.01 and 5.47 wt. %) with a mean of 1.42 wt. %; very low $Na_2O$ from 0.001 to 0.09 wt. % (with an average of 0.322 wt. %). There is very low concentration of $K_2O$ ranging from 0.017 to 0.04 wt. % with a mean of 0.016 wt. %; $P_2O_5$ are generally low with concentrations (0.0027 and 0.01 wt. %) with average of 0.0060 wt. %.
$SiO_2$ content >45 % is the upper limit for ultramafic rocks (Arndt *et al.,* 1977). The talcose rocks have affinity with the komatiite field (Fig. 8) of Jensen (1976). This is supported by the low concentrations of aluminum and potassium oxides, and the high magnesium content in the rocks. It also plots within the komatiitic field on $Al_2O_3$ vs. FeO/ (FeO + MgO) plot (Fig. 9). The talcose bodies therefore, most likely metamorphosed from a komatiite; an ultramafic mantle-derived volcanic rock. All the samples plot close on the talc field in the CaO-$SiO_2$-MgO plot (Fig. 10).

**Table 1: Chemical Compositions of Talcose Rock in the Study Area**

| Oxides/ Elements | TC 1 | TC 2 | TC 3 | TC 4 | TC 5 | TC 6 | TC 7 | TC 8 | TC 9 | TC 10 | TC 11 |
|---|---|---|---|---|---|---|---|---|---|---|---|
| $SiO_2$ | 60.94 | 61.69 | 58.39 | 61.04 | 61.69 | 60.76 | 59.33 | 60.42 | 58.16 | 57.96 | 61.01 |
| $TiO_2$ | 0.03 | 0.02 | 0.07 | 0.02 | 0.02 | 0.03 | 0.04 | 0.03 | 0.04 | 0.04 | 0.04 |
| $Al_2O_3$ | 0.82 | 0.37 | 1.86 | 0.56 | 0.47 | 0.59 | 2.68 | 1.46 | 1.84 | 1.9 | 0.58 |
| $Fe_2O_3$ | 4.38 | 3.95 | 5.73 | 4.29 | 4.25 | 4.71 | 5.62 | 4.82 | 5.71 | 5.46 | 4.24 |
| FeO | 3.4 | 3.07 | 4.45 | 3.33 | 3.3 | 3.66 | 4.36 | 3.75 | 4.44 | 4.24 | 3.3 |
| FeOt | 7.35 | 6.62 | 9.61 | 7.19 | 7.13 | 7.9 | 9.43 | 8.08 | 9.58 | 9.16 | 7.11 |

 

| | | | | | | | | | | | |
|---|---|---|---|---|---|---|---|---|---|---|---|
| **MnO** | 0.06 | 0.05 | 0.1 | 0.05 | 0.08 | 0.08 | 0.06 | 0.06 | 0.1 | 0.1 | 0.07 |
| **MgO** | 28.53 | 29.13 | 25.49 | 28.75 | 28.99 | 28.58 | 26.56 | 27.83 | 25.54 | 25.31 | 28.72 |
| **CaO** | 0.02 | 0.01 | 4.89 | 0.02 | 0.02 | 0.03 | 0.05 | 0.04 | 5.02 | 5.47 | 0.03 |
| **$Na_2O$** | 0.001 | 0.001 | 0.08 | 0.001 | 0.001 | 0.001 | 0.001 | 0.001 | 0.09 | 0.1 | 0.001 |
| **$Cr_2O_3$** | 0.75 | 0.87 | 0.29 | 0.95 | 0.21 | 0.8 | 0.66 | 0.65 | 0.33 | 0.3 | 0.71 |
| **K2O** | 0.02 | 0.0017 | 0.01 | 0.01 | 0.01 | 0.01 | 0.04 | 0.03 | 0.01 | 0.01 | 0.02 |
| **$P_2O_5$** | 0.01 | 0.0027 | 0.0027 | 0.0028 | 0.01 | 0.003 | 0.01 | 0.01 | 0.0029 | 0.0028 | 0.01 |
| **LOI** | 4.77 | 4.64 | 3.43 | 4.79 | 4.87 | 4.75 | 5.59 | 5.02 | 3.57 | 3.45 | 4.68 |
| **Ti** | 17.99 | 11.99 | 41.97 | 11.99 | 11.99 | 17.99 | 23.98 | 17.99 | 23.98 | 23.98 | 23.98 |
| **P** | 43.64 | 11.78 | 11.78 | 12.22 | 43.64 | 13.09 | 43.64 | 43.64 | 12.22 | 12.66 | 43.64 |
| **K** | 166.03 | 141.13 | 83.015 | 83.015 | 83.015 | 83.02 | 332.06 | 249.05 | 83.02 | 83.01 | 166.03 |
| **Sc** | 1.77 | 1.12 | 5.9 | 1.44 | 1.69 | 1.7 | 2.26 | 1.91 | 6 | 6.11 | 1.57 |
| **V** | 12.17 | 12.79 | 29.29 | 12.14 | 10.74 | 12.42 | 15.92 | 13.3 | 29.56 | 30.99 | 12.41 |
| **Cr** | 4197 | 4268 | 1981 | 4234 | 1181 | 4189 | 3680 | 3313 | 2201 | 2056 | 4296 |
| **Co** | 73.51 | 79.2 | 65.83 | 75.45 | 108.8 | 75.6 | 71.4 | 71.55 | 66.59 | 66.36 | 75.3 |
| **Ni** | 1980 | 2080 | 1334.2 | 2028 | 2065 | 1995 | 2118 | 2181 | 1393.8 | 1427 | 2083 |
| **Cu** | 3.92 | 6.16 | 6.77 | 3.23 | 3.7 | 5.66 | 7.08 | 4.11 | 7.77 | 9.32 | 3.58 |
| **Zn** | 109.1 | 104.2 | 70.6 | 108.3 | 57.6 | 111.8 | 92.7 | 87.2 | 72.9 | 68.5 | 113.4 |
| **Rb** | 1.17 | 0.356 | 0.357 | 0.96 | 0.506 | 0.945 | 2.8 | 2.26 | 0.291 | 0.263 | 1.27 |
| **Nb** | 0.95 | 0.42 | 0.5 | 0.62 | 0.66 | 0.7 | 3.68 | 1.9 | 0.51 | 0.51 | 0.63 |
| **Mo** | 0.315 | 0.36 | 0.36 | 0.31 | 0.27 | 0.271 | 0.42 | 0.51 | 0.43 | 0.35 | 0.4 |
| **Cs** | 0.15 | 0.15 | 0.06 | 0.17 | 0.14 | 0.17 | 0.44 | 0.21 | 0.05 | 0.03 | 0.14 |
| **Ba** | 4.8 | 5.21 | 11.4 | 4.93 | 4.96 | 4.72 | 5.6 | 5.81 | 9.17 | 11.12 | 4.75 |
| **Hf** | 0.03 | 0.02 | 0.06 | 0.02 | 0.05 | 0.03 | 0.08 | 0.07 | BDL | 0.02 | 0.05 |
| **Ta** | 0.17 | 0.04 | 0.04 | 0.09 | 0.07 | 0.09 | 0.66 | 0.35 | 0.04 | 0.04 | 0.08 |
| **Th** | 0.05 | 0.02 | 0.07 | 0.05 | 0.04 | 0.04 | 0.03 | 0.19 | 0.09 | 0.02 | 0.05 |
| **U** | 0.51 | 0.31 | 0.1 | 0.42 | 0.49 | 0.54 | 0.5 | 3.22 | 1.73 | 0.12 | 0.09 |
| **K/Rb** | 141.91 | 396.42 | 232.54 | 86.474 | 164.06 | 87.85 | 118.59 | 110.2 | 285.27 | 315.65 | 130.73 |
| **K/Sr** | 69.47 | 77.12 | 5.643 | 39.53 | 43.01 | 42.57 | 95.15 | 88.31 | 5.65 | 5.11 | 69.47 |

 

| | | | | | | | | | | | |
|---|---|---|---|---|---|---|---|---|---|---|---|
| **La** | 0.738 | 0.332 | 3.09 | 0.835 | 0.681 | 0.481 | 1.873 | 1.125 | 6.29 | 1.886 | 0.455 |
| **Ce** | 0.68 | 1.329 | 7.2 | 2.02 | 4.87 | 1.417 | 1.33 | 0.774 | 5.36 | 4.44 | 0.369 |
| **Pr** | 0.17 | 0.064 | 0.714 | 0.173 | 0.154 | 0.106 | 0.455 | 0.264 | 1.808 | 0.341 | 0.102 |
| **Nd** | 0.567 | 0.185 | 2.49 | 0.64 | 0.61 | 0.37 | 1.7 | 1.06 | 5.83 | 1.22 | 0.428 |
| **Sm** | 0.187 | 0.071 | 0.392 | 0.168 | 0.152 | 0.119 | 0.428 | 0.248 | 1 | 0.199 | 0.07 |
| **Eu** | 0.03 | 0.0076 | 0.154 | 0.028 | 0.039 | 0.023 | 0.091 | 0.047 | 0.279 | 0.11 | 0.032 |
| **Gd** | 0.184 | 0.05 | 0.251 | 0.141 | 0.13 | 0.115 | 0.474 | 0.294 | 0.62 | 0.2 | 0.134 |
| **Tb** | 0.0339 | 0.0086 | 0.0365 | 0.0229 | 0.019 | 0.019 | 0.09 | 0.047 | 0.066 | 0.0276 | 0.0239 |
| **Dy** | 0.193 | 0.044 | 0.32 | 0.108 | 0.142 | 0.119 | 0.388 | 0.311 | 0.405 | 0.178 | 0.105 |
| **Ho** | 0.039 | 0.007 | 0.057 | 0.03 | 0.022 | 0.027 | 0.075 | 0.054 | 0.076 | 0.043 | 0.021 |
| **Er** | 0.113 | 0.035 | 0.156 | 0.082 | 0.046 | 0.092 | 0.217 | 0.136 | 0.2 | 0.154 | 0.056 |
| **Tm** | 0.0187 | 0.0071 | 0.0218 | 0.0116 | 0.0095 | 0.015 | 0.038 | 0.0223 | 0.0197 | 0.0233 | 0.013 |
| **Yb** | 0.12 | 0.02 | 0.15 | 0.09 | 0.08 | 0.13 | 0.22 | 0.2 | 0.19 | 0.16 | 0.07 |
| **Lu** | 0.025 | 0.006 | 0.026 | 0.011 | 0.018 | 0.022 | 0.035 | 0.021 | 0.029 | 0.014 | 0.014 |
| **$La_N$** | 1.14 | 0.51 | 4.77 | 1.29 | 1.05 | 0.74 | 2.89 | 1.74 | 9.71 | 2.91 | 0.7 |
| **$Ce_N$** | 0.41 | 0.79 | 4.3 | 1.21 | 2.91 | 0.85 | 0.79 | 0.46 | 3.2 | 2.65 | 0.22 |
| **$Pr_N$** | 0.67 | 0.25 | 2.81 | 0.68 | 0.61 | 0.42 | 1.79 | 1.04 | 7.12 | 1.34 | 0.4 |
| **$Nd_N$** | 0.45 | 0.15 | 1.99 | 0.51 | 0.49 | 0.3 | 1.36 | 0.85 | 4.66 | 0.98 | 0.34 |
| **$Sm_N$** | 0.46 | 0.17 | 0.97 | 0.41 | 0.37 | 0.29 | 1.05 | 0.61 | 2.46 | 0.49 | 0.17 |
| **$Eu_N$** | 0.19 | 0.05 | 1 | 0.18 | 0.25 | 0.15 | 0.59 | 0.31 | 1.81 | 0.71 | 0.21 |
| **$Gd_N$** | 0.34 | 0.09 | 0.46 | 0.26 | 0.24 | 0.21 | 0.87 | 0.54 | 1.14 | 0.37 | 0.25 |
| **$Tb_N$** | 0.34 | 0.09 | 0.37 | 0.23 | 0.19 | 0.19 | 0.91 | 0.47 | 0.67 | 0.28 | 0.24 |
| **$Dy_N$** | 0.29 | 0.07 | 0.47 | 0.16 | 0.21 | 0.18 | 0.58 | 0.46 | 0.6 | 0.26 | 0.16 |
| **$Ho_N$** | 0.26 | 0.05 | 0.38 | 0.2 | 0.14 | 0.18 | 0.5 | 0.36 | 0.51 | 0.29 | 0.14 |
| **$Er_N$** | 0.26 | 0.08 | 0.36 | 0.19 | 0.11 | 0.21 | 0.5 | 0.31 | 0.46 | 0.35 | 0.13 |
| **$Tm_N$** | 0.28 | 0.1 | 0.32 | 0.17 | 0.14 | 0.22 | 0.56 | 0.33 | 0.29 | 0.34 | 0.19 |
| **$Yb_N$** | 0.26 | 0.03 | 0.34 | 0.19 | 0.19 | 0.3 | 0.51 | 0.46 | 0.43 | 0.36 | 0.17 |
| **$Lu_N$** | 0.37 | 0.09 | 0.39 | 0.16 | 0.26 | 0.32 | 0.52 | 0.31 | 0.43 | 0.21 | 0.21 |
| **Eu/Eu*** | 0.49 | 0.39 | 1.5 | 0.56 | 0.85 | 0.6 | 0.62 | 0.53 | 1.08 | 1.68 | 1.01 |

 

| | | | | | | | | | | | |
|---|---|---|---|---|---|---|---|---|---|---|---|
| $La_N/Yb_N$ | 4.37 | 15.06 | 13.93 | 6.69 | 5.58 | 2.5 | 5.69 | 3.77 | 22.77 | 8.12 | 4.24 |
| $La_N/Sm_N$ | 2.47 | 2.93 | 4.94 | 3.11 | 2.81 | 2.53 | 2.74 | 2.84 | 3.94 | 5.94 | 4.07 |
| $Ce_N/Yb_N$ | 1.56 | 23.33 | 12.55 | 6.26 | 15.45 | 2.85 | 1.56 | 1 | 7.51 | 7.4 | 1.33 |
| $Ce_N/Sm_N$ | 0.88 | 4.54 | 4.45 | 2.91 | 7.77 | 2.89 | 0.75 | 0.76 | 1.3 | 5.41 | 1.28 |

*Note: Oxides in wt. %, trace and rare earth elements in ppm. BDL: Below Detection Limit

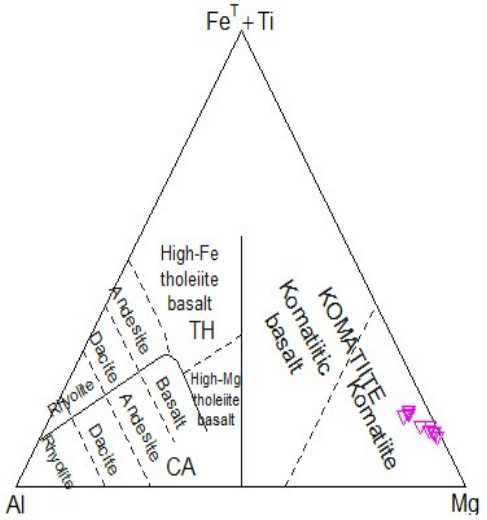


**Figure 8: Geotectonic Discrimination Plot of Talcose Rock in the Study Area (after Jensen, 1976; and modified from Jensen and Pyke, 1982)**

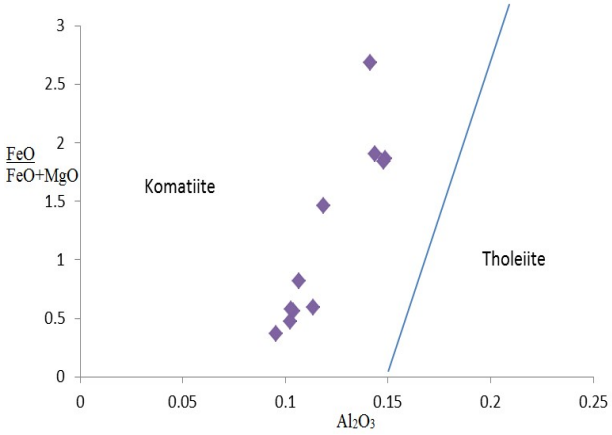


**Figure 9: Variation of $Al_2O_3$ with FeO/ (FeO + MgO) ratio in Ibogunde Talcose Rocks (Modified after Naldrett and Cabri, 1976)**

 

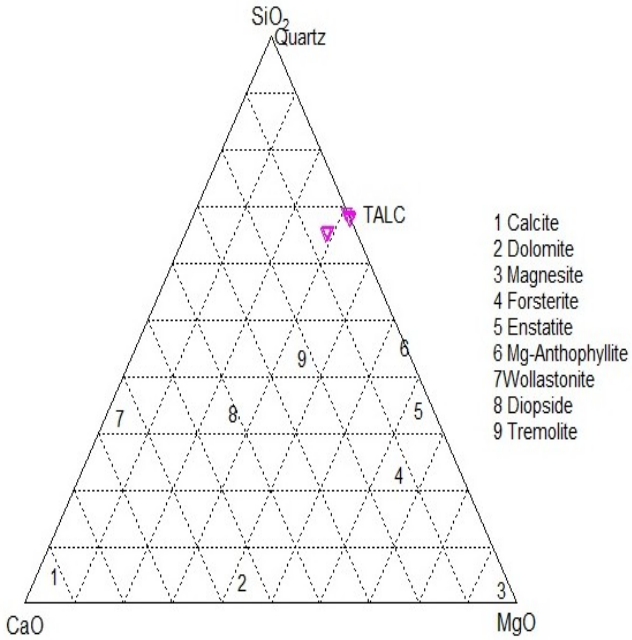


**Figure 10: CaO-$SiO_2$-MgO Plot for Talcose Rocks**

The trace element geochemical data showed that the concentrations of Ni (1334.2 - 2181 ppm) and Cr (1181 – 4296 ppm) are very high with average concentrations of 1880.45 and 3236 ppm, respectively. The rocks generally have low values for Ba (ranged from 4.72 to 11.4 ppm) and Rb (0.263 t0 2.8 ppm). Co and Zn have moderate concentrations (66.36 to 108.8 ppm and 57.6 - 113.4 ppm, respectively).

The ratios of $La_n/Yb_n$, $La_n/Sm_n$ and $Ce_n/Yb_n$ range from 2.5 to 22.77, 2.53 to 5.94 and 1 to 23.33, respectively. These ratios indicate fractionation of the source magma. The chondrite-normalized pattern shows no defined trend though the LREE is more enriched with depletion of HREE (Fig. 11). The HREE have very low concentration and reveal a flat plateau. The europium anomaly, Eu/Eu* is highly variable; ranged between 0.39 to 1.68 with a mean of 0.85. Eu* is the value obtained at the europium position by a straight-line interpolation between the plotted points for $Sm_n$ and $Gd_n$ using the chondrite normalized values. The REE pattern may be due to mobility of rare earth elements after the formation of the rock.

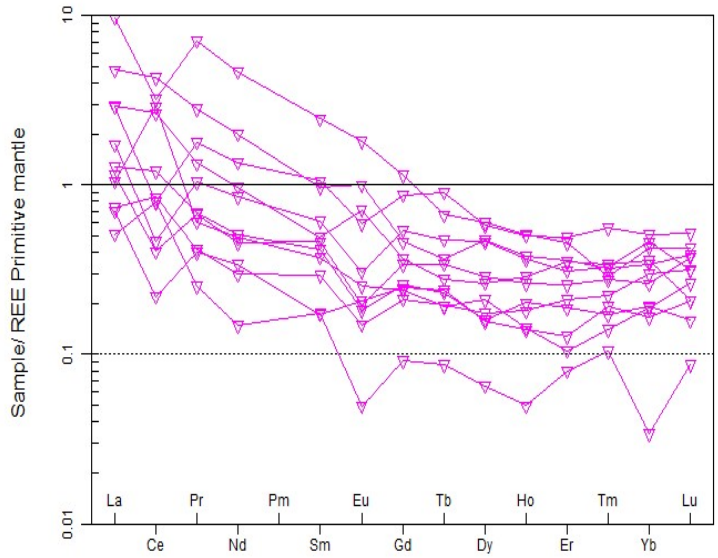


**Figure 11: Chondrite Normalized REE Diagram for Talcose Rock in the Study**

 

Five (5) samples of quartzite from the study area were analyzed for major, trace and rare earth elements. The results of the chemical analyses are presented in Tables 2a -2c. The rock is characterized by very high $SiO_2$ concentrations (97.56 to 99.44 wt. %) with an average of 98.54 wt. %; very low $TiO_2$ from 0.02 to 0.10 wt. % (with an average of 0.064 wt. %); low $Al_2O_3$ between 0.27 and 1.21 wt. % (mean of 0.73 wt. %); low $Fe_2O_3$ from 0.05 to 0.35 wt. % with an average of 0.18 wt. %. The rock generally has low CaO ranging between 0.01 and 0.02 wt. % with a mean of 0.0120 wt. %, low $Na_2O$ from 0.01 to 0.06 wt. % (with an average of 0.024 wt. %). The concentrations of $K_2O$ and $P_2O_5$ are generally low, ranging from 0.06 to 0.30 wt. % and 0.0001 to 0.01 wt. %, respectively, with mean values of 0.16 wt. % and 0.0040 wt. %, respectively. The concentrations of MgO and $Cr_2O3$ are below the detection limit. MnO has most concentrations to be below the level of detection with constant concentration value of 0.01 wt. %.
The geochemical data of quartzite showed that the trace elements generally have low concentrations except for K (498.09 to 2490.5 ppm). The concentrations of Ni range between 8 and 13.5 ppm; Cr concentration varies from 11.6 to 18.3 ppm. The values of Co range between 37.1 and 59.3 ppm with those of Zn ranging from 1.85 to 4.55 ppm.

The X-Ray diffractograms of ten (10) talcose samples were subdivided and stacked into three (3) groups of identical diffraction patterns (Figs. 12 a – c).
Group 1: TC 1, TC 2, TC 4, TC 6, TC 13
Group 2: TC 3, TC 9, TC 11
Group 3: TC 7, 8

The results of the X-ray diffraction analysis of the powdered talcose rocks showed peaks of talc, chlorite, tremolite. Other minor peaks include those of quartz and anthophyllite. The mineral assemblages for Group 1, 2, and 3 are talc, chlorite and anthophyllite; talc, quartz and anthophyllite; and talc, tremolite respectively (Figs. 12 a – c).

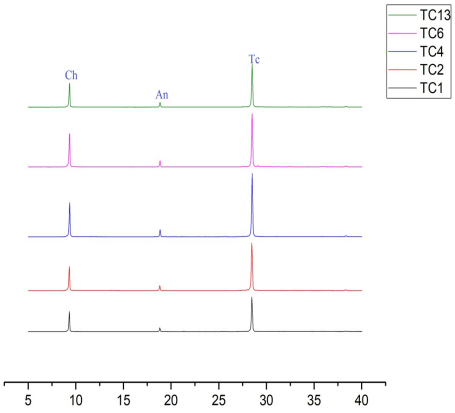


**Figure 12a: X-Ray Diffractograms of the Talcose Rocks for Group 1**
*Tc (Talc), Ch (chlorite) and An (Anthophyllite)

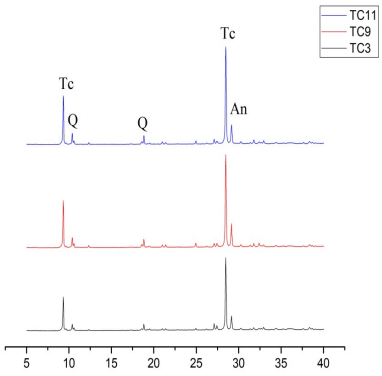


**Figure 12b: X-Ray Diffractograms of the Talcose Rocks for Group 2**

 

*Tc (Talc), Q (Quartz) and An (Anthophyllite)

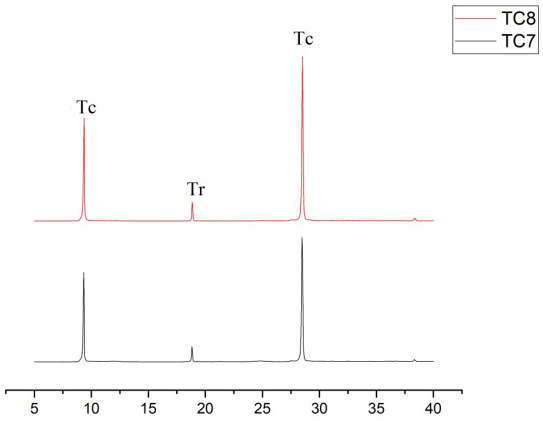


**Figure 12c: X-Ray Diffractograms of the Talcose Rocks for Group 3**

**Table 2a: Major Element Compositions of Quartzite in the Study Area (values in wt. %).**

| Sample No | $SiO_2$ | $TiO_2$ | $Al_2O_3$ | $Fe_2O_3$ | FeO | FeOt | MnO | CaO | $Na_2O$ | $K_2O$ | $P_2O_5$ | $Cr_2O_3$ |
|---|---|---|---|---|---|---|---|---|---|---|---|---|
| QTZ 1 | 97.97 | 0.04 | 1.21 | 0.09 | 0.06996 | 0.15094 | bdl | 0.02 | 0.06 | 0.2 | 0.01 | bdl |
| QTZ 2 | 98.95 | 0.1 | 0.31 | 0.18 | 0.13992 | 0.30188 | 0.01 | 0.01 | 0.01 | 0.07 | 0.0001 | bdl |
| QTZ 3 | 98.78 | 0.07 | 0.64 | 0.22 | 0.17101 | 0.36897 | 0.01 | 0.01 | 0.01 | 0.15 | 0.0001 | bdl |
| QTZ 4 | 97.56 | 0.09 | 1.21 | 0.35 | 0.27206 | 0.58699 | bdl | 0.01 | 0.03 | 0.3 | 0.01 | bdl |
| QTZ 5 | 99.44 | 0.02 | 0.27 | 0.05 | 0.03887 | 0.08386 | 0.01 | 0.01 | 0.01 | 0.06 | 0.0001 | bdl |

**Table 2b: Trace Element Compositions of Quartzite in the Study Area (values in ppm).**

| Sample No | K | Cr | Co | Ni | Cu | Zn | Rb | Nb | Mo | Cs | Ba | Pb | Th | U |
|---|---|---|---|---|---|---|---|---|---|---|---|---|---|---|
| QTZ 1 | 1660.3 | 16.8 | 37.1 | 13.5 | 4.55 | 5.9 | 8.43 | 1.99 | 1.06 | 0.42 | 55.3 | 5.97 | 1.84 | 0.73 |
| QTZ 2 | 581.11 | 18.3 | 48.4 | 9.2 | 3.49 | 4.4 | 2.36 | 4.65 | 1.54 | 0.15 | 21.9 | 1.84 | 1.85 | 0.42 |
| QTZ 3 | 1245.2 | 16.5 | 52.6 | 9.6 | 3.2 | 6.9 | 9.38 | 2.52 | 1.22 | 0.32 | 32.3 | 1.52 | 0.75 | 0.56 |
| QTZ 4 | 2490.5 | 17.4 | 53.6 | 9.2 | 3.9 | 12.9 | 28.1 | 6.07 | 1.09 | 0.58 | 76.8 | 2.45 | 1.83 | 1.05 |
| QTZ 5 | 498.09 | 11.6 | 59.3 | 8 | 1.85 | 6 | 1.5 | 0.8 | 0.85 | 0.23 | 28.8 | 1.01 | 2.63 | 0.42 |

 

**Table 2c: Rare Earth Element Compositions of Quartzite in the Study Area (values in ppm).**

| Sample No | La | Ce | Pr | Nd | Sm | Eu | Gd | Tb | Dy | Ho | Er | Tm | Yb | Lu | La/Yb | Ce/Yb |
|---|---|---|---|---|---|---|---|---|---|---|---|---|---|---|---|---|
| QTZ 1 | 10.65 | 14.69 | 2.01 | 6.07 | 1.23 | 0.26 | 0.9 | 0.15 | 0.66 | 0.16 | 0.246 | 0.08 | 0.24 | 0.08 | 44.2 | 61 |
| QTZ 2 | 6.08 | 12.25 | 1.23 | 4.42 | 0.68 | 0.13 | 0.54 | 0.11 | 0.32 | 0.08 | 0.14 | 0.06 | 0.16 | 0.06 | 39 | 78.5 |
| QTZ 3 | 2.38 | 5.42 | 0.533 | 1.84 | 0.415 | 0.06 | 0.26 | 0.06 | 0.25 | 0.05 | 0.173 | 0.07 | 0.16 | 0.05 | 15.2 | 34.5 |
| QTZ 4 | 4.28 | 10.06 | 0.901 | 3.12 | 0.64 | 0.2 | 0.5 | 0.1 | 0.4 | 0.16 | 0.243 | 0.08 | 0.32 | 0.09 | 13.4 | 31.5 |
| QTZ 5 | 8.21 | 15.8 | 1.7 | 6.52 | 1.09 | 0.14 | 0.75 | 0.12 | 0.56 | 0.13 | 0.26 | 0.07 | 0.21 | 0.09 | 40 | 77.1 |

Talc is the most abundant and predominant mineral with a mean percentage of 83.20% in all the ten samples (Table 3). The minerals identified corroborate the petrographic observations.

**Table 3: Mineralogical Compositions Based on X-Ray Diffraction Studies showing Relative Proportions of Minerals Present in Percentage**

| Minerals | Group 1 | Group 2 | Group 3 | Mean |
|---|---|---|---|---|
| Talc | 82.5 | 74.60 | 92.50 | 83.20 |
| Chlorite | 20.50 | - | - | 20.50 |
| Tremolite | - | - | 7.30 | 7.30 |
| Anthophyllite | 6.50 | 15.50 | - | 11.00 |
| Quartz | - | 10.00 | - | 10.00 |
| Total | 99.50 | 99.60 | 99.80 | |

## 5. DISCUSSIONS

Talc has been generally attributed to form from hydrothermal alteration of ultramafic rocks (Elueze and Ogunniyi, 1985; Ige, 1987; Adekoya, 1999). In rare cases, the high pressure metamorphism of quartzite under shearing can also lead to formation of talcose rock (Luzenac, 2004). About 10% of world production of talc can also be formed as a result of transformation of siliceous rocks such as quartzites, which provides the silica needed for the mineral's formation (Luzenac, 2003). Magnesium is brought by the migration of hydrothermal fluids. Owing to absence of ultramafic rock exposure in the vicinity of the study area, it is pertinent to compare the chemistry of quartzite (host) and talcose rocks to establish the genetic relationship or if otherwise.

The major element composition (Table 4) shows that quartzite is characterized by very high $SiO_2$ concentrations ranging from 97.56 to 99.44 wt. % with an average of 98.54 wt. % while talcose rock is characterized by small range of composition of $SiO_2$ between 57.96 and 61.69 wt. % (with mean of 60.118 wt. %). The $Al_2O_3$ mean values of quartzite and talc are 0.73 wt. % and 1.19 wt. %, respectively; $Fe_2O_3$ has averages of 0.18 wt. % and 4.83 wt. % for quartzite and talc, respectively. The average value for CaO in the quartzite and talc are 0.0120 wt. % and1.42 wt. %, respectively but both rocks have low average compositions of $Na_2O$ (0.024 wt. % and 0.322 wt. %). The concentrations of $K_2O$ and $P_2O_5$ with mean values of 0.16 wt. % and 0.004 wt. %, respectively in quartzite with averages of 0.016 wt. % and 0.0060 wt. %, respectively in talc. The concentrations of MgO and $Cr_2O_3$ are below the detection limit in quartzite but with mean value of 27.59 wt. %. and 0.593 wt. %, respectively in talc.

The trace and rare earth elements data of the quartzite reveals low concentration for Ni, Cr, Co and Zn (Tables 2b – 2c) while the talcose rock shows high abundance for Ni and Cr; moderate amount of Co and Zn (See Owoeye, 2020). The triangular diagram defined on the basis of millications classified the quartzite as having no affinity with komatiite series whereas the talcose rocks of Ibogunde area plot within the komatiite field (Fig. 13a) of Jensen (1976). Although, the talcose rocks are hosted by quartzite, there is no genetic affinity between these two rock types. The presence of chlorite, tremolite and anthophyllite as observed in the XRD and

 

petrographic studies further indicate an ultramafic origin of the talcose rock. The chondrite normalized REE diagram for both rocks also shows disparity in pattern (Fig. 13b).

**Table 4: Average Chemical Compositions of Talc and Quartzite in the Study Area**

| Oxides (%) | Talc (N =11) | Quartzite (N = 5) |
|---|---|---|
| $SiO_2$ | 60.118 | 98.54 |
| $Al_2O_3$ | 1.19 | 0.73 |
| $Fe_2O_3$ | 4.83 | 0.18 |
| CaO | 0.012 | 1.42 |
| NaO | 0.322 | 0.024 |
| $K_2O$ | 0.016 | 0.16 |
| $P_2O_5$ | 0.0060 | 0.004 |
| MgO | 27.59 | BDL |
| $Cr_2O_3$ | 0.593 | BDL |
| Ni | 1880.45 | 9.9 |
| Cr | 3236 | 16.12 |
| Co | 75.417 | 50.2 |
| Zn | 90.572 | 7.22 |

*Note: Oxides in wt. %, trace elements in ppm; BDL: Below Detection Limit; N = Number of samples

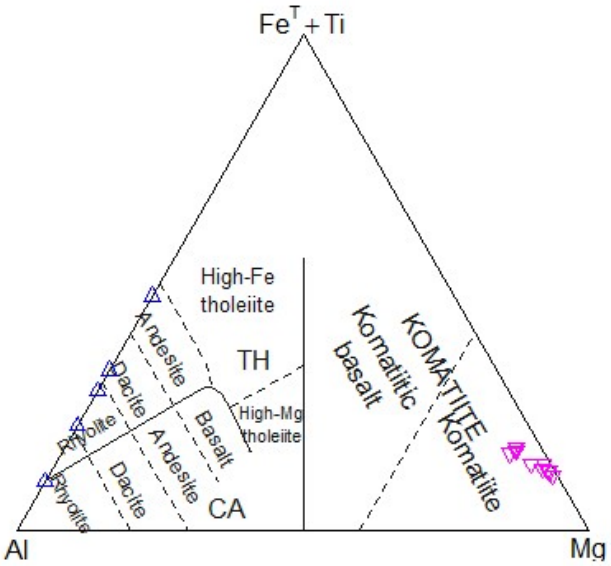


**Figure 13a: Geotectonic Discrimination Plot of Quartzite and Talcose Rock in the Study Area (After Jensen, 1976; modified by Jensen and Pyke, 1982)**

▲ Quartzite, ▽ Talc

 

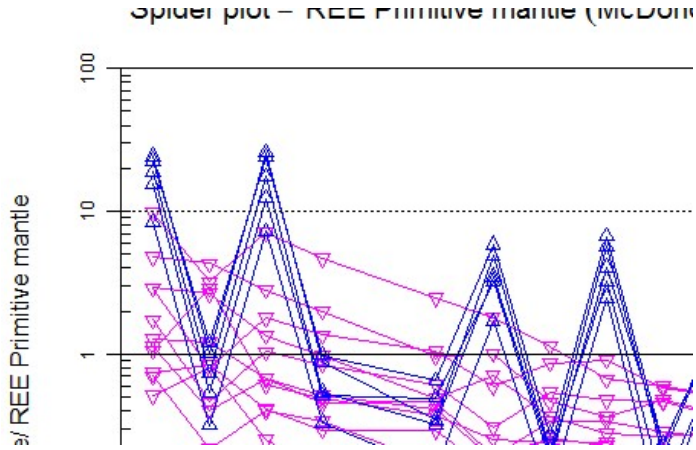


**Figure 13b: Chondrite Normalized REE Diagram for Talcose Rock and Quartzite in the Study Area (McDonough and Sun, 1995)**
*Blue Colour: Quartzite, Pink Colour: Talc

There is no geochemical relationship between talc and quartzite; the concentration values of the major, trace and rare earth elements are so far apart to deduce a common parentage for these rocks though field relationships exist between them. These observations show no genetic relationship between them in terms of petrogenesis and geotectonic classification.

## 6. CONCLUSIONS

Talcose rock occurs within the quartzite in the study area as separate and mappable bodies. Microscopically, the rock is composed predominantly of talc, chlorite and some opaque minerals. In addition to this, XRD revealed the presence of tremolite and anthophyllite. Talc has the most predominat peak and the most abundant mineral in all the ten samples.

The whole-rock geochemical data obtained have $SiO_2$, MgO, $Fe_2O_3$, CaO and $Al_2O_3$ as the major oxide compositions with $SiO_2$ having the highest average composition of 60.118 wt. $Na_2O$, $Cr_2O_3$, $P_2O_5$, MnO and $TiO_2$ account for less than 1 % of the bulk chemistry.

High concentrations of Ni and Cr may be as a result of immobility of Cr and Ni even under hydrothermal alteration. Low values of Ba and Rb are probably due to the chemical instability of these elements during secondary alteration. The REE ratios indicate fractionation of the source magma while the REE pattern may be due to mobility of rare earth elements after the formation of the rock.

The talcose rocks have affinity with the komatiite field as shown on the geotectonic discrimination plot after Jensen (1976) and variation of $Al_2O_3$ with FeO/ (FeO + MgO) as modified after Naldrett and Cabri (1976). The talcose bodies were therefore, most likely metamorphosed from a komatiite; an ultramafic mantle-derived volcanic rock. All the samples plot close on the talc field in the CaO-$SiO_2$-MgO plot.

The major peaks from the X-ray diffraction analysis of the talcose rocks were at talc, chlorite and tremolite. The most abundant and predominant mineral in all the ten samples was talc (Table 3). These minerals have petrographic features that are similar to talc in thin sections.

## ACKNOWLEDGEMENTS

This work is part of the first author's (Nee Owoeye) Ph. D thesis. Laboratory facilities were provided by the research visit facilitated by the third author while fourth author provided additional financial support. Ms. Mariella of the Central Analytical Facilities, Stellenbosch University made the analyses run smoothly despite her busy schedules.

## CONFLICT OF INTEREST

The authors declare that they have no conflict of interest.

Note: This work is part of the unpublished Ph.D. thesis of the first author who doubles as the corresponding author (formerly addressed as **Nee Owoeye**).

## REFERENCES

Adekoya, J. A. (1999) Rocks and Stones: Treasure house for national prosperity. Inaugural lecture series 19, delivered at Federal University of Technology Akure, 1, 32 – 33.

 

Adetunji, A., Olarewaju, V. O., Ocan, O. O., Ganev, V. Y. and Macheva, L. (2016) Geochemistry and U-Pb zircon geochronology of the pegmatites in Ede Area, Southwestern Nigeria: A newly discovered oldest Pan African rock in Southwestern Nigeria. *Journal of African Earth Sciences*, *115*: 177 – 190

Ajibade, A. C. (1976) Provisional classification and correlation of the schist belts in Northwest Nigeria. Kogbe, C. A. (Ed.) In: Geology of Nigeria. Elizabethan Publishing Company, Surulere, Lagos, Nigeria, 85 – 90.

Ajibade, A. C. and Wright, J. B. (1989) The Togo-Benin shield: evidence of crustal aggregation in the Pan-African belt. T*ectonophysics, 165*: 125 – 129.

Akin-Ojo, O. A. (1992) Compositional and industrial studies of talc bodies in the preCambrian domain of south western Nigeria. Unpublished Ph.D. Thesis University of Ibadan, 196 pp.

Alao-Daniel, A. B., Adetunji, A., Opuwari, M. A. and Eruteya, O. E. (2023) Integrated multielemental soil geochemical survey as a tool in geological mapping in the tropics: A case study of Songbe Area of Osun State, West Africa. *Journal of Environment and Earth Science*, 13 (5): 15 – 34.

Arndt, N. T., Naldrett, A. J. and Pyke, D. R. (1977) Komatiitic and iron rich tholeiitic lavas of Munro Township, Northeast Ontario. *Journal of Petrology*, *18*: 319 – 369.

Black, R., Latouche, L., Liegeois, J. P., Caby, R. and Bertrand, J. M. (1994) Pan African displaced terranes in the Tuareg shield (central Sahara). *Geology, 22*: 641 – 644.

Bolarinwa, A. T. (2001) Compositional and industrial evaluation of talc bodies of Oke-Ila area, Ilesha schist belt, South Western Nigeria, *Mineral Wealth Journal*, *118*: 89 – 100.

Bolarinwa, A. T. and Adeleye, M. (2015) Petrogenesis and functional applications of talcose rocks in Wonu-Apomu and Ilesa areas, Southwestern Nigeria. *Materials and Geoenvironment*, *62*: 81 – 93.

Caby, R. (1989) Precambrian terranes of Benin-Nigeria and Northeast Brazil and the late Proterozoic south Atlantic fit. *Geological Society of America*. Special paper 230: 145 – 158.

Darnley, A. G., Bjorklund, A., Bolviken, B., Gustavsson, N., Koval, P. V., Plant, J. A., Steenfelt, A., Tauchid, M., Xuejing, X., Garrett, R. G. and Hall, G. E. (1995) A global geochemical database for environmental and resource management. *Earth Science Report* 19, UNESCO Publishing, Paris, 22 – 23.

Durotoye, M. A. and Ige, O. A. (1991) An inventory of talc deposits in Nigeria and their industrial application potentials. *Journal of Mining and Geology. 27*(2): 27 – 31.

Elueze, A. A. and Ogunniyi, S. O. (1985) Appraisal of talc bodies of the Ilesha district, southwestern Nigeria and their potentials for industrial application. *Natural Resources Development*, 2221: 26 – 34.

Elueze, A. A. and Awonaiya, F. A. (1989) Investigation of talc bodies in Iseyin area, southwestern Nigeria in relation to their applications as industrial materials. *Journal of Mining and Geology*, *25*(2): 217 – 225.

Federal Survey of Nigeria (1965). 1:50,000 Topographical map of Iwo region, sheet 242 S.E. and NE.

Ferre, E., Deleris, J., Bouchez, J. L., Lar, A. U. and Peucat, J. J. (1996) The Pan-African reactivation of contrasted Eburnean and Archaean provinces in Nigeria. Structural and isotopic data: *Journal of the Geological Society, London, 153*: 719 – 728.

Ferre, E., Gleizes, G. and Caby, R. (2002) Obliquely convergent tectonics and granite emplacement in the Trans-Saharan belt of Eastern Nigeria: a synthesis. *Precambrian Research*, *114*: 199 – 219.

Hess, H. H. (1993) Hydrothermal metamorphism of an ultrabasic intrusion at Schuyler Virginia. *American Journal of Science*, *26*: 377 – 408.

Ige, O. A. (1987) Mineralogical and geochemical studies of some talc-bearing ultramafic and associated mafic rocks from Apomu and Ife-Ilesa Areas of Southwestern Nigeria. A published Ph.D. thesis of Obafemi Awolowo University, Ile-Ife, 220 pp.

Jensen, L. S. (1976) A new cation plot for classifying subalkalic volcanic rocks. Ontario Divisional Mines, Miscellaneous Paper, 66: 1 – 21.

Jensen, L. S. and Pyke, D. R. (1982) Komatiites in the Ontario portion of the Abitibi belt. Arndt, N. T. and Nisbet, E. G. (Ed.) In: Komatiites. Allen and Unwin, London, 5 – 11.

Jochum, K. P., Nohl, U., Herwig, K., Lammel, E., Stoll, B and Hofmann, A. W. (2005) GeoReM: A new geochemical database for reference materials and isotopic standards. *Geostandards and Geoanalytical Research*, *29*: 333 – 338.

Jochum, K. P., Weis, U., Stoll, B., Kuzmin, D., Yang, Q., Raczek, I., Jacob, D. E., Stracke, A., Birbaum, K., Frick, D. A., Günther, D. and Enzweiler, J. (2011) Determination of reference values for NIST SRM 610 617 Glasses Following ISO Guidelines. *Geostandards and Geoanalytical Research*, *35*: 397 – 429.

Jochum, K. P., Weis, U., Schwager, B., Stoll, B., Wilson, S. A., Haug, G. H., Andreae, M. O. and Enzweiler, J. (2016) Reference values following ISO guidelines for frequently requested rock reference materials. *Geostandards and Geoanalytical Research, 40*: 333 – 350.

Liegeois, J. P., Black, R., Navez, J. and Latouche, L. (1994) Early and late Pan-African orogenies in the Air assembly of terranes (Tuareg shield, Niger). *Precambrian Research, 67*: 59 – 88.

Luzenac Mines Limited (2003) Quarterly quality assessment report, Luzenac Mines. 6 pp.

Luzenac Mines Limited (2004) Talc for the world. http.www.luzenac.com, pp. 1 – 4.

 

Luzenac Mines Limited (2006) Quarterly quality assessment report, Luzenac Mines Number 215, 12 pp.

McCurry, P. (1976) The geology of the Precambrian to lower Paleozoic rocks of Northern Nigeria – a review. Kogbe, C. A. (Ed.) In: Geology of Nigeria (1st Edition). Elizabethan Publishing Company, Lagos, pp. 15 – 39.

McDonough, W. F. and Sun, S. (1995) The composition of the Earth. *Chemical Geology*, *120*: 223 – 253.

Naldrett, A. J. and Cabri, L. J. (1976) Ultramafic and Related Mafic Rocks: Their Classification and Genesis with Special Reference to the Concentration of Nickel Sulfides and Platinum-Group Elements. *Economic Geology*, *17*: 1131 – 1158.

Okunlola, O. A., Ogedengbe, O. and Ojutalayo, A. (2002) Compositional features and industrial appraisal of the Baba-Ode talc South Western Nigeria. *Global Journal of Geological Science, 1*(1), 63 – 72.

Okunlola, O. A., and Anikulapo, F. A. (2006) Compositional characteristics and industrial qualities of talcose rocks in Erin-Omu area, South Western Nigeria. *Journal of Mining and Geology*, *42*(2), 113 – 126.

Okunlola O. A., Akinola, O. O. and Olorunfemi, A. O. (2011) Petrochemical Characteristics and industrial features of talcose rock in Ijero-Ekiti area, Southwestern Nigeria. *Ife Journal of Science, 3*(2): 317 – 326.

Olajide-Kayode, J. O., Okunlola, O. A. and Olatunji, A. S. (2018) Compositional features and industrial assessment of talcose rocks of Itagunmodi-Igun Area, Southwestern Nigeria. *Journal of Geoscience and Environment Protection*, *6*: 59 – 77.

Olorunfemi, A. O., Olarewaju, V. O., Okunlola, O. A. and Adesiyan, T. A. (2009) Compositional features and industrial appraisal of talcose rock occurrence around Esie, Southwestern Nigeria. *Mineral Wealth*, *150*: 33 – 42.

Owoeye (2020) Geology and soil geochemistry of Ibogunde and its environs, Osun State, Southwestern Nigeria. Unpublished Ph.D Thesis. Obafemi Awolowo University, Ile-Ife, Osun State, Nigeria, 57 – 58, 94 – 100, 163 – 170.

Oyawoye, M. O. (1964) The Geology of the Nigeria Basement Complex. *Journal of Mining, Geological and Metallurgical Society*, *1*: 82 – 102.

Paton, C., Hellstrom, J., Paul, B., Woodhead, J. and Hergt, J. (2011) Iolite: freeware for the visualisation and processing of mass spectrometric data. *Journal of Analytical Atomic Spectrometry*, *26*: 2508 – 2518.

Rahaman, M. A. (1976) Review of the Basement geology of Southwestern Nigeria. Kogbe, C. A (Ed.) In: Geology of Nigeria. Elizabethan Publishing Company, Lagos, 41 – 58.

Rahaman, M. A. (1988) Recent advances in the study of the Basement Complex of Nigeria. Oluyide, P.O., Mbonu, W.C., Ogezi, A. E., Egbuniwe, I. G., Ajibade, A. C. and Umeji, A. C. (Eds.) In: Precambrian Geology of Nigeria, Geological Survey of Nigeria, 11 – 41.

Turner, D. C. (1983) Upper Proterozoic Schist Belts in the Nigerian sector of the Pan-African province of West Africa. *Precambrian Research*, *21*: 55 – 79.